Identifying Dominant Drivers of Wind Erosion and Assessing Ecological Risk on the Qinghai-Tibet Plateau Using an XGBoost-SHAP Model

Shuliang Ouyang[1,2,3], Yujian Zhong [2,3], Xia Zhao [2,3,4*], Kelong Chen [2,3,4,5], Yong Shi [2,3] and Yu Zhou [2,3]

[1]College of Life Science, Qinghai Normal University, Xining 810008, China
[2]Qinghai Provincial Key Laboratory of Physical Geography and Environmental Process, College of Geographical Science, Qinghai Normal University, Xining 810008, China
[3]Key Laboratory of Tibetan Plateau Land Surface Processes and Ecological Conservation (Ministry of Education), Qinghai Normal University, Xining 810008, China
[4]Academy of Plateau Science and Sustainability, People's Government of Qinghai Province and Beijing Normal University, Xining 810008, China
[5]National Positioning Observation and Research Station of Qinghai Lake Wetland Ecosystem, Xining 810008, China

Abstract. Wind erosion is a key pathway of land degradation in the alpine drylands of the Qinghai-Tibet Plateau, yet its dominant controls and risk trajectories remain difficult to attribute in a spatially heterogeneous system. Here we integrated the RWEQ with an interpretable machine learning framework (XGBoost coupled with SHAP) to quantify spatiotemporal patterns of potential wind erosion from 1981 to 2020, identify dominant drivers, and delineate management-oriented ecological risk zones. The Plateau-wide mean potential wind erosion modulus was 3.03×10^4 t/km^2, with localized hotspots up to 1.08×10^5 t/km^2. Wind erosion showed strong seasonality, with most losses occurring from late winter to spring, and a predominantly declining long-term tendency that was spatially heterogeneous across climate classes. SHAP interpretation ranked erosive wind speed as the leading control (mean(|SHAP|) = 10.28), followed by sand content (5.17) and fractional vegetation cover (4.05), with elevation and soil organic matter as secondary modifiers. Dominant driver mapping attributed 59.69% of the Plateau to wind dominance, 9.96% to sand dominance, and 4.49% to vegetation dominance, while 24.74% was non-erosive. Risk zoning indicated extensive recovery areas (54.01%) and substantial gradually worsening belts (17.73%), with rapid worsening hotspots concentrated in wind driven zones (3.33%). The proposed RWEQ plus XGBoost-SHAP framework provides a transparent basis for prioritizing monitoring and targeted mitigation under climate variability.

1 Introduction

Wind erosion represents one of the most pervasive pathways of land degradation in dryland environments. By detaching and transporting fine surface particles, it removes nutrient-rich topsoil, weakens soil functioning, and reduces the capacity of land to sustain vegetation and agricultural production[1]. Its impacts are not confined to the land surface itself. Wind-eroded sediments and dust can deteriorate air quality, disrupt transportation, and increase environmental and public health risks across downwind regions[2]. In the context of climate change, these concerns have become more pressing, because shifts in wind regimes, moisture conditions, and vegetation cover may substantially alter the magnitude and distribution of wind erosion[3]. The Qinghai-Tibet Plateau is highly relevant in this regard. As an ecologically strategic region with extensive alpine drylands and fragile surface environments, it is exceptionally sensitive to climatic fluctuations[4]. While the southeastern Plateau is comparatively humid and less prone to severe wind erosion, large parts of the central, western, and northern Plateau are characterized by sparse vegetation, unconsolidated surface materials, and strong aeolian forcing, creating favorable conditions for erosion to occur[5]. Examining wind erosion across the Qinghai-Tibet Plateau is therefore important for understanding land degradation processes in climate-sensitive highland systems and for supporting ecological protection in this critical region.

Despite substantial progress in wind erosion assessment, identifying the dominant drivers of wind erosion change remains methodologically challenging. Wind erosion results from the combined influence of climatic factors, vegetation conditions, soil properties, and land-surface characteristics, and these controls often operate in nonlinear and spatially heterogeneous ways[6]. Previous studies have commonly relied on correlation analysis, regression-based interpretation, or factor-detection approaches such as geographic detectors to infer the roles of different variables[7]. These methods are informative for describing statistical associations, yet they

* Corresponding author: zhaoxia-qh@163.com

are less effective when the objective is to disentangle complex nonlinear responses, quantify the relative contribution of multiple predictors, and reveal how driver importance varies across space[8]. Interpretable machine learning offers a useful way forward. In particular, the combination of XGBoost (eXtreme Gradient Boosting) and SHAP (SHapley Additive exPlanations) makes it possible to couple strong predictive capacity with transparent model interpretation[9]. This framework can rank predictor importance, explain marginal effects, and support the identification of dominant controls in complex environmental systems[10]. For wind erosion studies on the Qinghai-Tibet Plateau, such an approach is especially valuable because it helps move beyond simple factor screening toward a more process-informed understanding of the spatial patterns and underlying causes of wind erosion change.

In this context, the present study integrates the Revised Wind Erosion Equation (RWEQ) with an interpretable machine learning framework based on XGBoost and SHAP to investigate wind erosion and its ecological risk on the Qinghai-Tibet Plateau. The objectives of this study are to: (1) characterize the spatiotemporal patterns of wind erosion on the Qinghai-Tibet Plateau from 1981 to 2020 using the RWEQ model; (2) identify the dominant drivers of wind erosion change and quantify their relative importance using the XGBoost-SHAP framework; and (3) delineate ecological risk zones for wind erosion to provide a scientific basis for regional ecological conservation and targeted risk management under climate change.

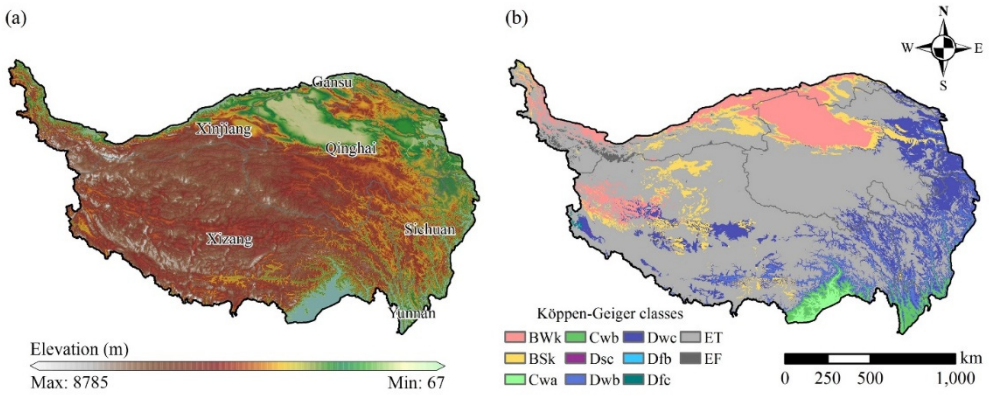

Figure 1 Topographic and climatic setting of the Qinghai-Tibet Plateau: (a) elevation; (b) Köppen Geiger climate classes[11]. In panel (b), abbreviations denote BWk, arid desert cold; BSk, arid steppe cold; Cwa, temperate dry winter hot summer; Cwb, temperate dry winter warm summer; Dsc, cold dry summer cold summer; Dwb, cold dry winter warm summer; Dwc, cold dry winter cold summer; Dfb, cold no dry season warm summer; Dfc, cold no dry season cold summer; ET, polar tundra; EF, polar frost.

2 Materials and methods

2.1 Study Area

The Qinghai-Tibet Plateau is the largest plateau in China and the highest on Earth, often referred to as the "Roof of the World"[12]. It extends from 26°00′ to 39°47′ N and 73°19′ to 104°47′ E, covering approximately 2.5 million km^2, which accounts for nearly one-quarter of China's total land area. The Plateau encompasses the Tibet Autonomous Region and Qinghai Province, and extends into adjacent parts of Xinjiang, Gansu, Sichuan, and Yunnan (Fig. 1a). Characterized by pronounced topographic heterogeneity and steep elevation gradients, the Plateau's strong relief, together with complex land surface conditions, creates sharp spatial gradients in temperature, moisture availability, vegetation cover, and near-surface wind environments[13]. This makes it a representative highland system for investigating wind erosion and its associated ecological risks.

Climatically, the Plateau spans multiple Köppen-Geiger climate classes (Fig. 1b), reflecting a transition from the relatively warm and humid southeastern margin to the cold and arid interior and high mountain environments. Temperate monsoon-influenced zones (Cwa, Cwb) occur mainly along the southeastern and southern margins. Cold and dry climates dominate large portions of the central and northern Plateau, including BSk and BWk, along with cold continental types characterized by winter dryness (Dwb, Dwc). Cold climates without a dry season (Dfb, Dfc) occur in areas with relatively higher moisture supply, while high-elevation tundra and ice cap environments are represented by ET and EF. The Plateau experiences relatively high annual mean near-surface wind speeds, generally ranging from 0.6 to 4.2 m/s, with maxima in spring and minima in autumn[14]. A significant declining trend in wind speed has been observed in recent decades[15]. Precipitation is strongly seasonal, mainly concentrated between June and September, broadly coinciding with the warm season[16].

2.2 Data Sources and Preprocessing

To support RWEQ-based estimates of wind erosion for 1981-2020, we assembled meteorological, soil property, and auxiliary datasets. Meteorological inputs included daily mean air temperature, daily precipitation, daily mean downward shortwave radiation, and hourly wind speed. Soil variables comprised sand, silt, and clay contents, soil organic carbo, and calcium carbonate. Auxiliary datasets included daily snow depth, a digital elevation model (DEM), and a 16-day NDVI product used to characterize vegetation cover. Prior to factor derivation,

all gridded layers were reprojected, clipped, and resampled to a common grid to ensure spatial consistency. Continuous variables were resampled using bilinear interpolation, whereas categorical variables were resampled using nearest-neighbor assignment[17]. Temporal harmonization was conducted to align datasets with the daily time step required by the RWEQ calculations. Data sources and key attributes are summarized in Table 1.

$$U_{2m} = U_{10m}\left(\frac{2}{10}\right)^{\frac{1}{7}} \quad (1)$$

Where, U_{2m} and U_{10m} are the wind speeds at heights of 2 m and 10 m, respectively (m/s).

$$\rho = 348\left(\frac{1.013 - 0.1183EL + 0.0048EL^2}{273.15 + t}\right) \quad (2)$$

Where, EL is elevation (km), t is air temperature (°C), and ρ is air density (kg/m^3).

Given the strong environmental heterogeneity of the Qinghai-Tibet Plateau, several targeted preprocessing steps were applied when deriving RWEQ factors[18]. First, hourly wind speed at 10 m was converted to the 2 m height required by RWEQ using the 1/7 power-law profile (Eq. 1). To better represent erosive wind conditions, the wind factor was computed from the intra-day hourly wind series rather than from daily mean wind speed, with the threshold friction condition represented by a wind-speed threshold of 5 m/s. Second, air density was calculated as a spatially varying field from elevation and air temperature (Eq. 2), avoiding the use of a single constant and better accounting for the Plateau's large elevational gradients[19]. Third, the soil moisture factor relied on potential evaporation estimated from shortwave radiation and air temperature[20]. When daily mean temperature was ≤ -17.8 °C, potential evaporation was set to zero, and the moisture factor was assigned as zero to prevent nonphysical values and to reflect negligible wind erosion under extreme cold conditions. Fourth, the snow cover factor was implemented as a daily binary constraint: SD was set to 0 when snow depth was ≥ 25.4 mm and to 1 otherwise. Fifth, soil properties from the 0-5, 5-15, and 15-30 cm layers were combined as a depth-weighted mean to represent the 0-30 cm layer used in model calculations. Finally, NDVI was converted to fractional vegetation cover using the pixel dichotomy approach[21]; missing pixels were filled with zero, and NDVI for 1981 was replaced with the nearest available record (1982).

Table 1 Data sources and descriptions used in this study.

Factor	Variables	Resolution	Sources
Meteorology	Air temperature	1/30°, daily	CMFD: China meteorological forcing dataset v2.0 [22]
Meteorology	Wind speed	1/30°, hourly	
Meteorology	Precipitation	1/30°, daily	
Meteorology	Downward shortwave radiation	1/30°, daily	
Soil Properties	Sand, Silt, Clay	1 km	Harmonized World Soil Database v2.0[23]
Soil Properties	SOC	1 km	
Soil Properties	$CaCO_3$	1 km	
Topography	DEM	1 km	WorldClim v2.1[24]
Surface Conditions	Snow depth	0.25°, daily	Long-term series of daily snow depth dataset in China[25]
Surface Conditions	NDVI	1/12°, 16-day	PKU GIMMS NDVI Dataset[26]

2.3 Revised Wind Erosion Equation

The Revised Wind Erosion Equation (RWEQ) is a widely used empirical framework for estimating wind-driven soil loss, with its formulation rooted in the WEQ family of models developed from early wind erosion research[27]. In RWEQ, wind erosivity and surface protection are represented through a set of multiplicative factors describing atmospheric conditions, soil susceptibility, surface roughness, and vegetation shielding, which makes the model well suited for gridded applications when field observations are sparse. Although initially designed with cropland conditions in mind, RWEQ has been increasingly applied in large-area assessments and multi-decadal analyses by coupling the model with remote sensing and reanalysis products[28,29]. RWEQ has been applied to characterize the spatial patterns of wind erosion and to inform assessments of aeolian land degradation and the effectiveness of wind erosion mitigation measures[30]. The general form of the RWEQ model is given as follows:

$$Q_{max} = 109.8(\mathrm{WF} \cdot \mathrm{EF} \cdot \mathrm{SCF} \cdot \mathrm{K'} \cdot \mathrm{COG}) \quad (3)$$

$$S = 150.71(\mathrm{WF} \cdot \mathrm{EF} \cdot \mathrm{SCF} \cdot \mathrm{K'} \cdot \mathrm{COG})^{-0.3711} \quad (4)$$

$$S_L = \frac{2z}{S^2} Q_{max} e^{-\left(\frac{z}{S}\right)^2} \quad (5)$$

Where Q_{max} is the maximum transport capacity (kg/m), S is the critical field length (m), S_L is the soil loss (kg/m^2), and z is the downwind distance (m), which was set to 50 m in this study. In Eqs. (3) - (5), WF, EF, SCF, K', and COG denote the climatic factor (kg/m), soil erodibility factor (dimensionless), soil crust factor (dimensionless), surface roughness factor (dimensionless), and combined vegetation factor (dimensionless), respectively. The calculation of these factors is described in Eqs. (6) - (16).

$$WF = W_f \cdot \frac{\rho}{g} \cdot \mathrm{SW} \cdot \mathrm{SD} \quad (6)$$

$$W_f = \frac{\sum_{i=1}^{N} U_2(U_2 - U_1)^2}{N} \times N_d \quad (7)$$

$$SW = \frac{ET_P - (R + I)\frac{R_d}{N_d}}{ET_P} \quad (8)$$

$$ET_P = 0.0162\left(\frac{SR}{58.5}\right)(DT + 17.8) \quad (9)$$

$$SD = 1 - P(snowcover \geq 25.4mm) \quad (10)$$

WF reflects how erosive winds are amplified or suppressed by atmospheric density as well as by surface wetness and snow cover, which limit particle detachment and transport. Accordingly, higher *WF* indicates more favorable climatic conditions for wind-driven soil loss.

Where W_f is the wind factor (m^3/s^3), U_2 is the wind speed at 2 m height (m/s), U_1 is the threshold wind speed at 2 m (m/s) (below which W_f is set to 0; set to 5 m/s in the study), N_d is the length of the wind-speed observation period (days) (set to 1 day), N is the number of wind-speed records within the observation period (set to 1), ρ is air density (kg/m^3), g is gravitational acceleration (m/s^2) (set to 9.8 m/s^2), SW is the soil moisture factor (dimensionless), SR is total solar radiation (cal/cm^2), DT is mean air temperature (°C), ET_p is potential evaporation (mm), I is irrigation amount (mm) (set to 0), R_d is the number of days with rainfall and irrigation (days) (approximated by the number of rainy days in this study), and *SD* is the snow cover factor (dimensionless).

$$EF_1 = \frac{29.09 + 0.31Sa + 0.17Si}{100} \quad (11a)$$

$$EF_2 = \frac{0.33\left(\frac{Sa}{cl}\right)}{100} \quad (11b)$$

$$EF_3 = \frac{2.59OM + 0.95CaCO_3}{100} \quad (11c)$$

$$EF = EF_1 + EF_2 - EF_3 \quad (11c)$$

$$SCF = \frac{1}{1 + 0.0066cl^2 + 0.021OM^2} \quad (12)$$

EF and *SCF* describe the intrinsic susceptibility of the soil surface to wind erosion and the extent to which the surface is protected by crusting. *EF* represents the erodibility of the soil, integrating the effects of texture and key soil constituents that influence particle detachability. *SCF* characterizes the stabilizing effect of soil crusts, which can increase surface resistance and reduce the likelihood of particle entrainment; lower *SCF* therefore indicates stronger crust protection.

Where *cl*, *Si*, and *Sa* are the clay, silt, and sand contents, respectively (% by weight), *OM* is soil organic matter content (% by weight), and $CaCO_3$ is calcium carbonate content (% by weight).

$$K' = e^{\left(1.88K_r - 2.44K_r^{0.934} - 0.124C_{rr}\right)} \quad (13)$$

$$K_r = 0.2\frac{(\Delta H)^2}{L} \quad (14)$$

K' represents the surface roughness effect in RWEQ and reflects how terrain-induced roughness modifies near-surface airflow and, in turn, the potential for particle detachment and transport. Greater roughness generally reduces wind erosivity at the soil surface by increasing drag and disrupting wind flow, thereby suppressing wind erosion. In this study, ridge roughness was approximated using local relief to make this factor applicable to the complex natural terrain of the Qinghai-Tibet Plateau[31].

Where K_r is ridge roughness (m), ΔH is the elevation difference within a window of length L (m), L is the relief length scale (m), and C_{rr} is the random roughness factor (cm). In this study, K_r was approximated by the local relief; ΔH values greater than 158 m were capped at 158 m to avoid nonphysical behavior; L was set to 270 m (a 3×3 neighborhood of the 90 m DEM).

$$COG = e^{-5.614(CC^{0.7366})} \quad (15)$$

$$CC = \frac{NDVI - NDVI_{soil}}{NDVI_{veg} - NDVI_{soil}} \quad (16)$$

COG captures the protective effect of vegetation on wind erosion and was parameterized using vegetation cover derived from *NDVI*. Residue-related terms in the original RWEQ formulation were omitted due to data limitations.

Where *CC* is canopy cover (%) and is approximated by fractional vegetation cover in this study; *NDVI* is the normalized difference vegetation index; and $NDVI_{veg}$ and $NDVI_{soil}$ are the *NDVI* values representing full vegetation cover and bare soil, defined as the 95th and 5th percentiles of *NDVI*, respectively. The residue-related terms *SC* (flat residue cover, %) and *SA* (standing stem area index) were not included due to limited data availability.

2.4 An Interpretable Machine Learning Framework Based on XGBoost and SHAP

Capturing the nonlinear responses of wind erosion to multiple environmental controls, together with their interactions, is difficult for conventional statistical approaches that rely on linearity assumptions or require interactions to be specified a priori. We therefore adopted XGBoost (eXtreme Gradient Boosting), a scalable gradient-boosted decision-tree algorithm that iteratively builds an ensemble of trees to reduce prediction error. Through regularization and shrinkage, XGBoost controls model complexity and tends to generalize well in high-dimensional settings with correlated predictors[32,33]. These properties make it well suited for heterogeneous landscapes such as the Qinghai-Tibet Plateau, where wind erosion is shaped by complex, spatially varying relationships with its drivers. In this study, XGBoost was trained using gridded environmental covariates and RWEQ-derived wind erosion estimates to generate spatially continuous predictions, providing the modeling backbone for subsequent SHAP-based attribution and effect interpretation. A high-level schematic diagram illustrating the full analytical framework of RWEQ integration with XGBoost-SHAP, and the subsequent steps for dominant driver mapping and ecological risk zoning is provided in Figure 2.

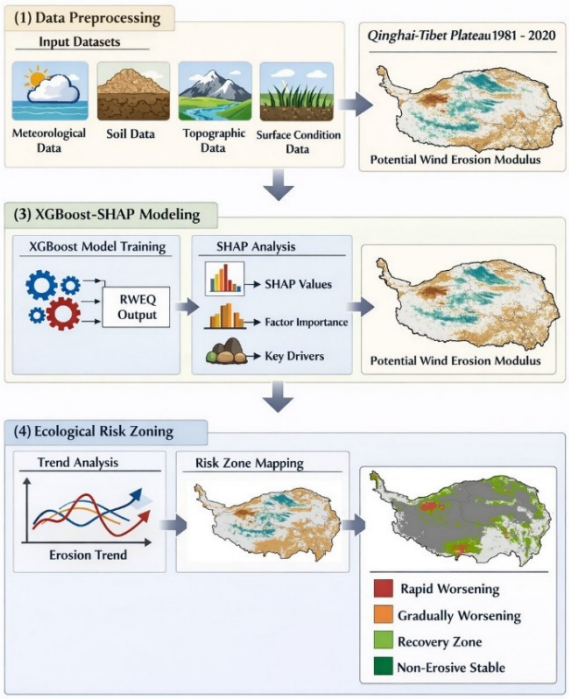

Figure 2 Schematic diagram of the integrated RWEQ-XGBoost-SHAP analytical framework

The framework consists of four core steps: (1) Data preprocessing: harmonizing meteorological, soil, topographic and surface condition datasets to a consistent spatial-temporal resolution for model input; (2) RWEQ simulation: calculating the potential wind erosion modulus across the Qinghai-Tibet Plateau from 1981 to 2020 by quantifying climatic, soil erodibility, surface roughness and vegetation protection factors; (3) XGBoost-SHAP modeling: training the XGBoost model with environmental covariates and RWEQ-derived potential wind erosion as the response variable, then using SHAP values to quantify factor importance and identify dominant drivers of wind erosion; (4) Ecological risk zoning: integrating dominant driver classes and the long-term trend of potential wind erosion to delineate management-oriented ecological risk zones, with differentiation of rapid worsening, gradually worsening, recovery and non-erosive stable zones.

To interpret the fitted model, we adopted SHAP (SHapley Additive exPlanations), an attribution approach grounded in Shapley values from cooperative game theory. SHAP decomposes a model prediction into additive contributions from individual predictors, allowing consistent interpretation at both the global scale (importance ranking) and the sample scale (dependence patterns and conditional effects)[34]. Here, SHAP values were computed from the trained XGBoost model to quantify each factor's contribution to wind erosion variation and to identify dominant drivers, which were further summarized as importance rankings and dependence relationships.

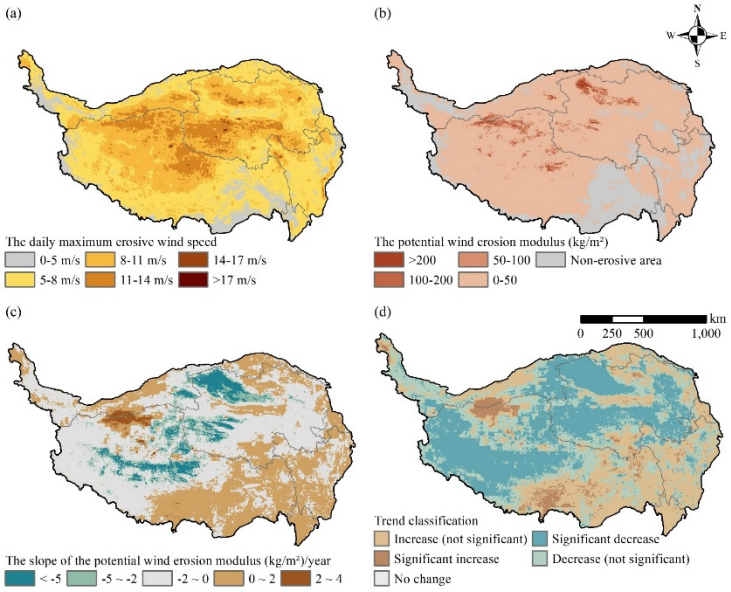

Figure 3 Spatial patterns and long-term trends of potential wind erosion on the Qinghai-Tibet Plateau: (a) spatial distribution of the daily maximum erosive wind speed in 2020; (b) spatial distribution of the potential wind erosion modulus in 2020; (c) interannual trend (slope) of the potential wind erosion modulus during 1981-2020, estimated as the pixel-wise slope from an ordinary least squares linear regression; (d) statistical significance of the trend in panel (c) based on a t-test at α=0.05.

3 Results

3.1 Spatiotemporal Patterns of Wind Erosion on the Qinghai-Tibet Plateau from 1981 to 2020

The modeling results indicate that the mean potential wind erosion modulus over the Qinghai-Tibet Plateau is 3.03×10^4 t/km^2, with localized hotspots reaching up to 1.08×10^5 t/km^2. The daily maximum erosive wind speed in 2020 exhibits clear spatial contrasts, with extensive areas dominated by moderate classes and distinct hotspots reaching the highest wind-speed bins in the Plateau's arid and sparsely vegetated regions (Fig.3a). Consistent with this wind regime, the 2020 potential wind erosion modulus shows a strongly clustered spatial pattern (Fig.

3b). High erosion intensities are concentrated in dryland sectors where surface materials are loose and vegetation protection is limited, whereas large portions of the Plateau are mapped as non-erosive or low erosion, indicating that erosive wind conditions and surface susceptibility do not co-occur uniformly in space. The long-term trend maps further reveal a spatially heterogeneous evolution of wind erosion between 1981 and 2020 (Fig. 3c, d). Most pixels show negative slopes, and the trend classification indicates that decreasing classes account for a broad share of the Plateau, with many areas reaching statistical significance at α=0.05. Patches of positive slopes persist in some regions, forming localized increasing zones that are mainly classified as non-significant increases, with fewer areas showing significant increases. Overall, the Plateau-wide pattern is dominated by decreases, while increases are spatially limited and fragmented.

Temporal dynamics derived from Figure 4 show pronounced seasonality and a weakening long-term tendency at the Plateau scale. The intra-annual allocation of annual wind erosion is highly uneven (Fig. 4a). Wind erosion is concentrated in late winter and spring, with the largest contributions occurring from February to April and a peak in early spring. Contributions decline sharply toward summer, reaching minima during July to August, and then recover toward late autumn and early winter. This seasonal pattern is consistent with periods of stronger winds and lower surface protection during the cold season and spring transition. At the interannual scale, the Plateau-wide annual potential wind erosion modulus exhibits substantial variability, together with an overall declining tendency during 1981-2020 (Fig. 4b). The ordinary least squares fit yields a negative slope, with year-to-year fluctuations superimposed on the long-term decrease. Several years stand out as anomalously low or high relative to the fitted trend, indicating that episodic climatic conditions can modulate wind erosion intensity even under a decreasing background tendency.

Climate-stratified results show that trend direction and magnitude differ systematically among Köppen-Geiger classes (Fig. 4c). The ET zone occupies the largest area share (62.17%) and shows a negative mean slope of about -0.51 (kg/m^2)/year, with decreasing categories collectively accounting for most of its area. The arid classes BWk (10.76%) and BSk (6.90%) exhibit stronger decreases, with mean slopes of about -2.93 and -1.14 (kg/m^2)/year, respectively, and large fractions classified as significant decreases. Dwc (12.76%) also shows a clear negative mean slope of about -0.84 (kg/m^2)/year. In contrast, Dwb (3.45%) is characterized by a near neutral to slightly positive mean slope of about 0.04 (kg/m^2)/year, with most pixels falling into increasing categories, mainly non-significant increases. The "Other" class (3.96%) displays an overall near zero mean slope. These results indicate that the strongest declines are concentrated in arid and cold climates, whereas weak increases are more likely to occur within specific continental climate settings.

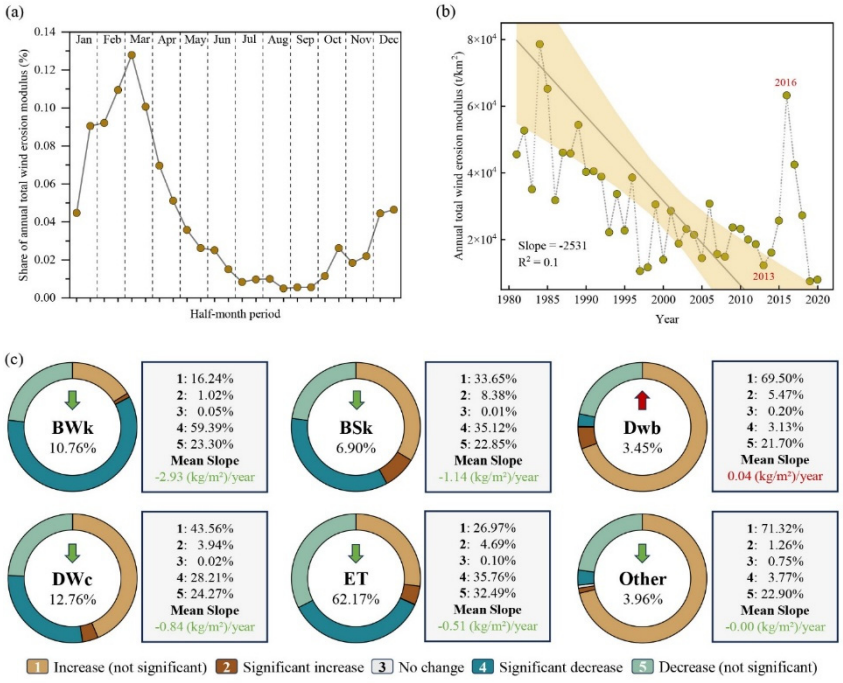

Figure 4 Seasonal distribution, interannual variability, and climate-specific trends of potential wind erosion on the Qinghai-Tibet Plateau: (a) intra-annual allocation of the annual total potential wind erosion modulus during 1981-2020, expressed as the share contributed by each half-month period (ID 1-24), calculated by summing gridded half-month values across years for the same period and converting the multi-year totals to percentages; (b) interannual variations in the plateau-wide annual potential wind erosion modulus during 1981-2020, with an ordinary least squares linear trend and its 95% confidence interval; (c) climate-stratified statistics of pixel-wise trend (slope) in potential wind erosion modulus during 1981-2020 for six climate groups, where donut charts show the area shares of five trend-significance categories (significant increase, non-significant increase, no change, significant decrease, and non-significant decrease); the center labels indicate the areal proportion of each climate group across the plateau; arrows denote the overall direction of change (green downward for decreasing; red upward for increasing); and the boxed values report category-specific area percentages and the mean slope for each climate group. Statistical significance is based on a t-test at α=0.05.

3.2 Feature Importance Analysis Using XGBoost-SHAP

We used SHAP to interpret the XGBoost model and quantify the relative importance of environmental controls on potential wind erosion across the Qinghai–Tibet Plateau (Fig. 5). At the plateau scale, Wind is the dominant predictor, with a mean(|SHAP|) of 10.28, clearly exceeding the next-ranked factors Sand (5.17) and FVC (4.05). Terrain and soil properties form a secondary tier, led by DEM (2.51) and SOM (2.08), whereas SnowD, AI, and Srad contribute more modestly (all ~1-1.5). Prcp and Temp show weaker overall influence (<1), and $CaCO_3$, Clay, and Silt have the smallest contributions.

Beyond rank order, the SHAP summary distribution indicates consistent directional patterns for key drivers. Higher Wind and Sand values are predominantly associated with positive SHAP values, implying increased predicted wind erosion, while higher FVC generally shifts SHAP values negative, reflecting the protective role of vegetation cover. Several predictors exhibit mixed positive and negative effects across samples, consistent with non-linear responses and interaction effects captured by XGBoost.

Climate stratification reveals that the relative importance of predictors is not spatially uniform (Fig. 5b-g). In the two arid classes (BWk and BSk), Wind remains overwhelmingly influential and the contributions of Sand, FVC, and DEM are comparatively amplified, consistent with strong exposure and high surface erodibility. In ET (tundra), the importance structure becomes more balanced, where Wind still ranks first but Sand and FVC approach comparable influence, and DEM and SnowD contribute as additional modifiers. In contrast, Dwb and the "Other" group show near-zero mean(|SHAP|) for most variables, which aligns with their very low mean erosion levels and indicates limited model sensitivity within these subsets.

Overall, the XGBoost-SHAP results emphasize a plateau-wide hierarchy in which erosive wind forcing sets the primary potential for wind erosion, while surface texture and vegetation cover regulate susceptibility, and topographic and cryo-climatic factors modulate this susceptibility in a climate-dependent manner.

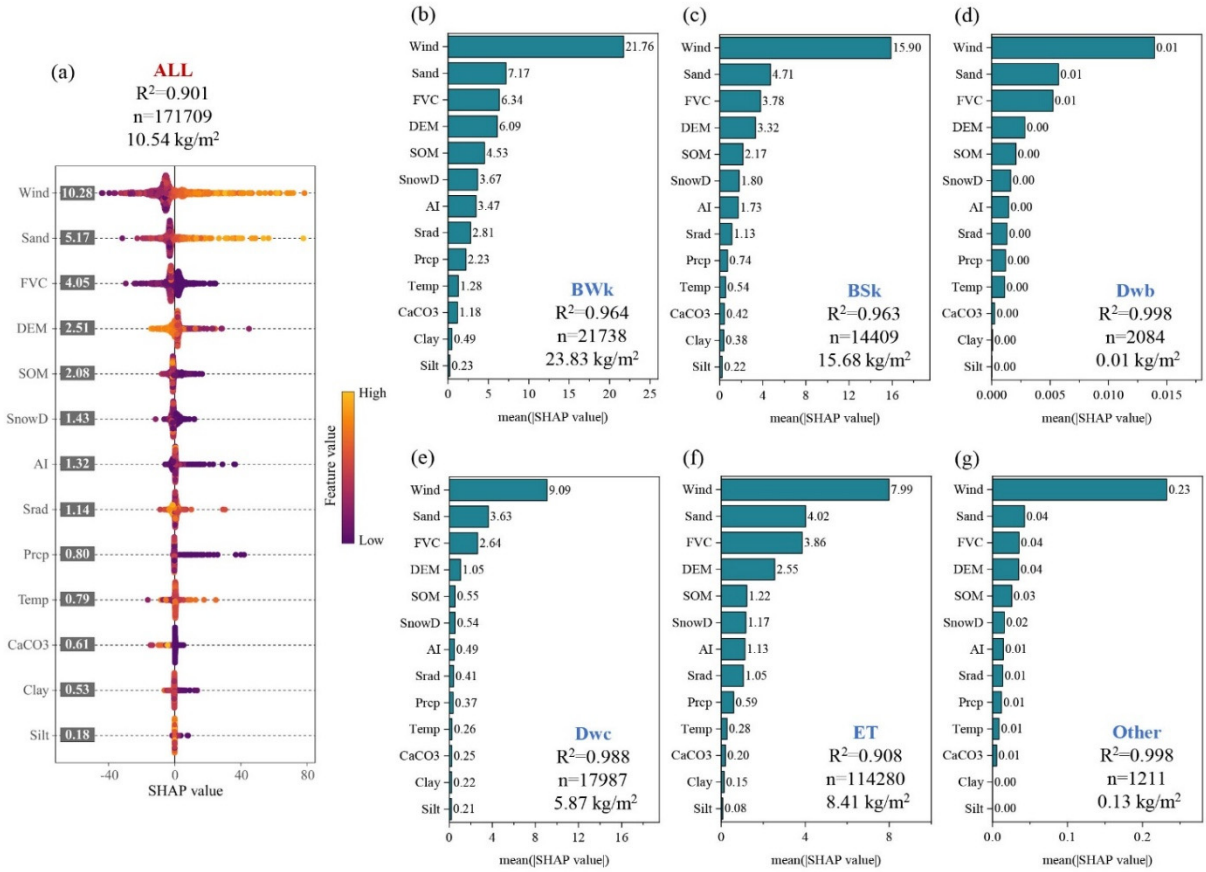

Figure 5 SHAP-based analysis of factors influencing potential wind erosion on the Qinghai–Tibet Plateau: (a) SHAP summary (beeswarm) plot showing the distribution of feature effects and the corresponding mean(|SHAP|)-based importance ranking; (b-g) climate-stratified feature importance rankings (mean(|SHAP|)) for BWk, BSk, Dwb, Dwc, ET, and Other. In panel (a), SHAP values indicate the direction and magnitude of each predictor's contribution to the XGBoost prediction (positive values increase and negative values decrease the predicted wind erosion modulus), and point colors denote feature values from low to high; the numbers beside feature names report mean absolute SHAP values. Each panel reports the model performance (R^2), sample size (n), and the mean wind erosion modulus (kg/m^2) for the corresponding domain. Predictor abbreviations are Wind, erosive wind speed; Sand, sand content; FVC, fractional vegetation cover; DEM, elevation from the digital elevation model; SOM, soil organic matter; SnowD, snow depth; AI, aridity index; Srad, solar radiation; Prcp, precipitation; Temp, air temperature; $CaCO_3$, calcium carbonate content; Clay, clay content; and Silt, silt content.

3.3 Identification and Spatial Characterization of Dominant Drivers of Wind Erosion Change

The dominant drivers of wind erosion change, identified by the leading SHAP contributor, show clear spatial contrasts across the Qinghai-Tibet Plateau (Fig. 6a). Erosive wind speed dominates most extensively, accounting for 59.69% of the plateau and forming a broadly continuous pattern across large parts of the western and central Plateau. Sand content is the second-most prevalent driver (9.96%), occurring mainly as clustered patches that coincide with sandy surfaces and aeolian deposits, particularly in arid and semi-arid sectors. Areas where fractional vegetation cover dominates are more localized (4.49%), appearing as belts and mosaics in transitional zones where vegetation gradients are pronounced. Regions dominated by other factors are limited (1.12%) and occur as small, scattered patches, indicating that secondary controls only locally outweigh the primary wind and surface constraints. In addition, 24.74% of the plateau is classified as non-erosive, concentrated mainly along the more humid southeastern margin and other well-protected areas where erosive conditions are not met.

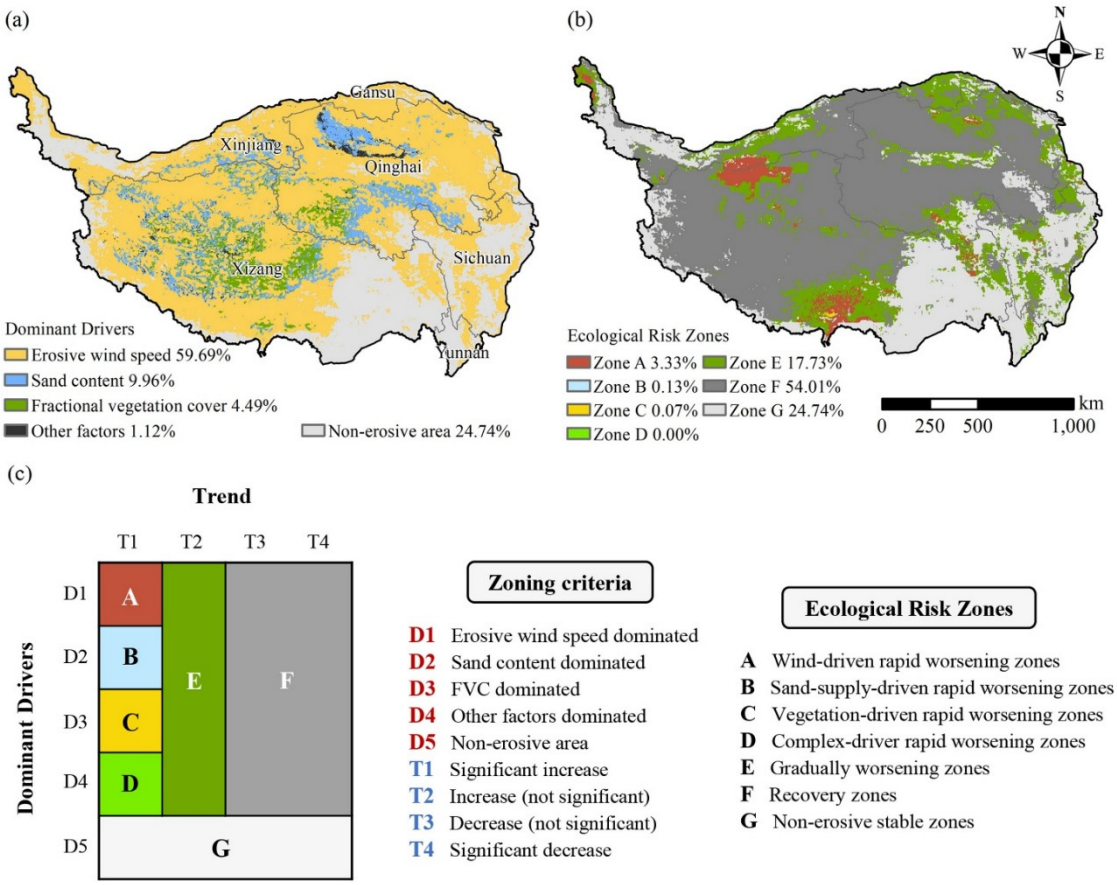

Figure 6 Ecological risk zoning of potential wind erosion on the Qinghai-Tibet Plateau based on dominant drivers and long-term trends: (a) spatial distribution of dominant drivers identified by the leading SHAP contributor from the XGBoost model, including erosive wind speed, sand content, fractional vegetation cover, and other factors, with the non-erosive area shown separately; (b) resulting ecological risk management zones (Zones A-G) derived from the integrated zoning criteria; (c) schematic of the zoning scheme combining dominant-driver classes (D1-D5) and trend categories (T1-T4) to define Zones A-G.

3.4 Ecological Risk Zoning

For ecological risk zoning, we developed a management-oriented scheme by integrating the dominant drivers of potential wind erosion with the multi-decadal trend in wind erosion during 1981-2020. Each grid cell was first assigned a dominant-driver type based on the leading SHAP contributor from the XGBoost model, including erosive wind speed, sand content, fractional vegetation cover , and other factors (Fig. 6a). Trend categories were derived from the direction and statistical significance of the 1981-2020 change (Fig. 3d). Because areas classified as “no change” were largely confined to non-erosive regions, they were not further partitioned in the risk zoning. We then delineated seven risk management zones that prioritize both risk trajectory and actionable controls (Fig. 6c). Areas with significant increases in wind erosion were subdivided by dominant drivers into four high-risk zones: (A) wind-driven rapid worsening, (B) sand-supply-driven rapid worsening, (C) vegetation-driven rapid worsening, and (D) complex-driver rapid worsening dominated by other factors. Areas showing increasing but non-significant trends were grouped as (E) gradually worsening zones, representing early warning areas where prevention-oriented management is warranted. Areas with decreasing trends, regardless of significance, were

grouped as (F) recovery zones, where the focus is on consolidating improvements and preventing rebound. Finally, (G) non-erosive stable zones were defined as areas lacking erosive conditions.

The resulting ecological risk zones exhibit pronounced spatial clustering across the Plateau (Fig. 6b). Recovery zones (Zone F) dominate the landscape, accounting for 54.01% of the Plateau, and form a broadly continuous swath across much of the interior Plateau. Gradually worsening zones (Zone E) occupy 17.73% and occur mainly as patchy belts around the margins of the recovery-dominated core, highlighting areas where wind erosion shows an upward tendency and warrants preventive management. Non-erosive stable zones (Zone G) comprise 24.74% and are concentrated primarily along the relatively humid southeastern margin and other sheltered areas where erosive conditions are not met. Among the rapid-worsening high-risk zones, Zone A (wind-driven) is the most extensive (3.33%) and appears as clustered hotspots, whereas Zones B (0.13%) and C (0.07%) are spatially limited and occur as small, isolated patches. Zone D is negligible in areal extent (0.00% after rounding), indicating that areas where "other factors" dominate significant increases are rare at the Plateau scale.

4 Discussion

4.1 Implications of Wind Erosion Driving Mechanisms for Ecological Risk Management

Wind forcing emerged as the primary control on potential wind erosion across the Plateau, consistent with the physics of wind-driven particle entrainment and transport and the broader environmental consequences of dust emission [35]. It is important to note that the potential wind erosion modulus simulated by RWEQ in this study is a model-derived index reflecting the erosive potential of the surface, which is a function of climatic conditions, soil properties and vegetation cover, rather than a directly validated measurement of actual aeolian sediment fluxes or dust emission mass in the field. This dominance also underscores the management relevance of seasonality, with late winter to spring concentrating the annual erosion signal, and of multi-decadal variability in near-surface winds, including documented stilling and possible recovery phases that can reshape risk trajectories [36].

The secondary importance of sand content indicates that many hotspots are constrained by sediment availability as well as wind energy, implying a shift in management emphasis depending on whether the system is wind-limited or supply-limited. Where sand-dominated patches occur, interventions should prioritize source control and disturbance minimization to reduce loose material availability and prevent expansion of exposed sandy surfaces, including those associated with lake retreat and newly exposed shorelines[37].

Vegetation protection, captured by fractional vegetation cover, generally reduced modeled erosion, supporting restoration and grazing management as practical levers in transitional areas where cover changes are most consequential[38]. Because the protective effect can be nonlinear and sensitive to spatial configuration, measures that improve cover continuity along dominant wind corridors and maintain effective surface shielding during the non-growing season are likely to yield disproportionate benefits, especially where NDVI-based proxies under-represent non-photosynthetic vegetation and residue protection[39].

The proposed risk zoning translates these mechanisms into differential priorities: rapidly worsening zones warrant immediate, targeted action; gradually worsening zones function as early warning areas where low-cost prevention and intensified monitoring are justified; recovery zones call for consolidation to avoid rebound. Interpretable machine learning strengthens this pathway by using XGBoost for robust prediction and SHAP for transparent attribution, enabling dominant driver maps to guide monitoring design, evaluate interventions, and update zoning as wind regimes and surface conditions evolve[40]. While the modelled potential wind erosion captures the key environmental controls of actual aeolian processes, direct field observations of sediment fluxes would further validate the magnitude of erosion and refine the risk zoning framework for the Qinghai-Tibet Plateau.

4.2 Limitations and Future Perspectives

Uncertainty in this study stems from both model structure and input data. Although RWEQ enables multi-decadal assessments at regional scale, it simplifies several processes that are likely important on the Qinghai-Tibet Plateau, including freeze and thaw controls on surface erodibility and other daily scale dynamics such as short-term changes in roughness[41]. Vegetation shielding was derived from NDVI, which can miss non-photosynthetic vegetation and surface residues during the non-growing season and may therefore underestimate protective effects[42]. The meteorological forcing and long-term NDVI products provide spatially complete coverage, yet their resolution and error structures propagate into gridded erosion estimates, especially in terrain with sharp elevational gradient[22]. In addition, soil attributes were treated as static, even though frozen ground processes and selective loss of fine particles can alter texture and aggregate stability through time[43]. Future work should integrate non-photosynthetic vegetation or residue metrics, deploy ground observations of aeolian fluxes and particle concentrations in key dust source areas for validation, and explicitly incorporate decadal near-surface wind variability and potential recovery when updating dynamic risk zoning[44].

5 Conclusion

This study combined RWEQ with an interpretable XGBoost-SHAP framework to map potential wind erosion across the Qinghai-Tibet Plateau for 1981-2020, quantify nonlinear driver contributions, and translate mechanism understanding into ecological risk zoning. Potential wind erosion was highly clustered, with a Plateau-wide mean of 3.03×10^4 t/km^2 and localized maxima reaching 1.08×10^5 t/km^2. Wind erosion exhibited

pronounced seasonality, concentrating in late winter and spring, and showed an overall declining tendency over the past four decades while retaining localized increasing areas.

Model interpretation identified a clear driver hierarchy. Erosive wind speed exerted the strongest control on erosion variability, while sand content and fractional vegetation cover regulated susceptibility through sediment availability and surface protection. The dominant driver map further indicated that wind-limited conditions prevail across most of the interior Plateau, whereas supply-related and vegetation-related controls occur as spatially coherent patches, providing actionable targets for differentiated management.

By integrating dominant drivers with trend significance, the proposed zoning scheme distinguished rapid worsening hotspots, gradually worsening early warning belts, recovery zones, and non-erosive stable areas. These outputs support a management strategy that emphasizes regional monitoring and early warning in wind-dominated areas, source control in sand-dominated patches, and restoration and grazing management in vegetation-sensitive transition zones, while consolidating gains in recovery regions. Overall, the study demonstrates that coupling process-based wind erosion estimation with transparent machine learning attribution can strengthen mechanism-based risk management and enable iterative updating of priority zones as climatic forcing and surface conditions evolve.

References

1. Klink, Carlos Augusto C, and Ricardo B. R Machado. "Conservation of the Brazilian Cerrado." Conservation Biology 19, no. 3 (2005): 707-713. https://doi.org/10.1111/j.1523-1739.2005.00702.x.
2. Leung, Danny M. D, et al.. "A new process-based and scale-aware desert dust emission scheme for global climate models – Part II: Evaluation in the Community Earth System Model version 2 (CESM2)." Atmospheric chemistry and physics 24, no. 4 (2024): 2287-2318. https://doi.org/10.5194/acp-24-2287-2024.
3. Ravi S, Breshears D D, Huxman T E, et al. Land degradation in drylands: Interactions among hydrologic-aeolian erosion and vegetation dynamics[J]. Geomorphology, 2010, 116(3-4): 236-245, https://doi.org/10.1016/j.geomorph.2009.11.023.
4. Li L H, Zhang Y L, Wu J S, et al. Increasing sensitivity of alpine grasslands to climate variability along an elevational gradient on the Qinghai-Tibet Plateau[J]. Science of the Total Environment, 2019, 678: 21-29, https://doi.org/10.1016/j.scitotenv.2019.04.399.
5. Teng Y M, Zhan J Y, Liu W, et al. Spatiotemporal dynamics and drivers of wind erosion on the Qinghai-Tibet Plateau, China[J]. Ecological Indicators, 2021, 123: 107340, https://doi.org/10.1016/j.ecolind.2021.107340.
6. Duniway M C, Pfennigwerth A A, Fick S E, et al. Wind erosion and dust from US drylands: a review of causes, consequences, and solutions in a changing world[J]. Ecosphere, 2019, 10(3): e02650, https://doi.org/10.1002/ecs2.2650.
7. Fan, Kaixuan K, et al.. "Assessing the relative contribution of climate change and human activity factors to spatiotemporal distributions of sand fixation service in the Loess Plateau." GIScience & Remote Sensing 62, no. 1 (2024). https://doi.org/10.1080/15481603.2024.2444630.
8. Alonso-González, Esteban E, et al.. "The snow cover is more important than other climatic variables on the prediction of vegetation dynamics in the Pyrenees (1981-2014)." Environmental Research Letters 19, no. 6 (2024): 064058-064058. https://doi.org/10.1088/1748-9326/ad4e4c.
9. Li, Ziqi Z. "Extracting spatial effects from machine learning model using local interpretation method: An example of SHAP and XGBoost." Computers Environment and Urban Systems 96 (2022): 101845-101845. https://doi.org/10.1016/j.compenvurbsys.2022.101845.
10. Zhang, Junyi J, et al.. "Insights into geospatial heterogeneity of landslide susceptibility based on the SHAP-XGBoost model." Journal of environmental management 332 (2023): 117357. https://doi.org/10.1016/j.jenvman.2023.117357.
11. Beck, H., Zimmermann, N., McVicar, T. et al. Present and future Köppen-Geiger climate classification maps at 1-km resolution. Sci Data 5, 180214 (2018). https://doi.org/10.1038/sdata.2018.214.
12. Li, Huan H, et al.. "Environmental filtering increases with elevation for the assembly of gut microbiota in wild pikas." Microbial biotechnology 12, no. 5 (2019): 976-992. https://doi.org/10.1111/1751-7915.13450.
13. Li, Yuefeng Y, et al.. "Control of local topography and surface patterning on the formation and stability of a slope permafrost peatland at 4800-m elevation on the central Qinghai-Tibetan Plateau." Ecological Indicators 158 (2023): 111475-111475. https://doi.org/10.1016/j.ecolind.2023.111475.
14. Lin, Di-an D, et al.. "Variability of soil organic carbon with elevation gradient in the Yarlung Tsangpo River Basin on the southeastern Tibetan Plateau." International Soil and Water Conservation Research 13, no. 4 (2025): 945-956. https://doi.org/10.1016/j.iswcr.2025.06.005.
15. Wu, Shaohong S, Yunhe Y Yin, Zheng Z Du, and Yang Y Qinye. "Climatic trends over the Tibetan Plateau during 1971–2000." Journal of Geographical Sciences 17, no. 2 (2007): 141-151. https://doi.org/10.1007/s11442-007-0141-7.
16. Liu, Xiaodong X, Aijuan A Bai, and Changhai C Liu. "Diurnal variations of summertime precipitation over the Tibetan Plateau in relation to orographically-induced regional circulations." Environmental Research Letters 4, no. 4 (2009): 045203-045203. https://doi.org/10.1088/1748-9326/4/4/045203.
17. Hall, Jaclyn M JM, et al.. "Scaling categorical spatial data for earth systems models." Global change biology 21, no. 1 (2015): 1-3. https://doi.org/10.1111/gcb.12708.
18. Yang, Dazhi D, and Yaqun Y Liu. "Heterogeneous impacts of human activities and climate change on transformed vegetation dynamics on the Qinghai-Tibet Plateau." Journal of environmental management 392 (2025): 126575. https://doi.org/10.1016/j.jenvman.2025.126575.
19. Yuan, Hongyu H, Taoyong T Su, Guoqiang G Li, and Kewei K Li. "Numerical simulation investigation on aerodynamic characteristics of rotor in plateau environment." Aerospace Science and Technology 155 (2024): 109628-109628. https://doi.org/10.1016/j.ast.2024.109628.
20. Yin, Ziyun Z, et al.. "A synthesis of Global Streamflow Characteristics, Hydrometeorology, and Catchment

Attributes (GSHA) for large sample river-centric studies." Earth system science data 16, no. 3 (2024): 1559-1587. https://doi.org/10.5194/essd-16-1559-2024.

21. Jiapaer, Guli G, Xi X Chen, and Anming A Bao. "A comparison of methods for estimating fractional vegetation cover in arid regions." Agricultural and Forest Meteorology 151, no. 12 (2011): 1698-1710. https://doi.org/10.1016/j.agrformet.2011.07.004.
22. He, J., Yang, K., Tang, W. Lu, H., Qin, J., Chen, Y.Y., & Li, X. (2020). The first high-resolution meteorological forcing dataset for land process studies over China. Scientific Data, 7, 25, https://doi.org/10.1038/s41597-020-0369-y.
23. FAO & IIASA. 2023. Harmonized World Soil Database version 2.0. Rome and Laxenburg. DOI: 10.4060/cc3823en.
24. Fick, S.E. and R.J. Hijmans, 2017. WorldClim 2: new 1km spatial resolution climate surfaces for global land areas. International Journal of Climatology 37 (12): 4302-4315.
25. Che, T., Dai, L., Li, X. (2015). Long-term series of daily snow depth dataset in China (1979-2024). National Tibetan Plateau Third Pole Environment Data Center. https://doi.org/10.11888/Geogra.tpdc.270194.
26. Li, M., Cao, S., Zhu, Z., Wang, Z., Myneni, R. B., and Piao, S.: Spatiotemporally consistent global dataset of the GIMMS Normalized Difference Vegetation Index (PKU GIMMS NDVI) from 1982 to 2022, Earth Syst. Sci. Data, 15, 4181–4203, https://doi.org/10.5194/essd-15-4181-2023, 2023.
27. Zhang, Gangfeng G, et al.. "An increase in wind erosion dominated by wind speed changes over the Tibetan Plateau from 1982 to 2020." The Science of the total environment 998 (2025): 180278. https://doi.org/10.1016/j.scitotenv.2025.180278.
28. Sun, Ranhao R, et al.. "Global Wind Erosion Reduction Driven by Changing Climate and Land Use." Earth s Future 12, no. 10 (2024). https://doi.org/10.1029/2024ef004930.
29. Li, Jiangyue J, Xiaofei X Ma, and Chi C Zhang. "Predicting the spatiotemporal variation in soil wind erosion across Central Asia in response to climate change in the 21st century." The Science of the total environment 709 (2020): 136060. https://doi.org/10.1016/j.scitotenv.2019.136060.
30. Liao, Jie J, et al.. "No increase of soil wind erosion with the establishment of center pivot irrigation system in Mu-Us sandy land." The Science of the total environment 939 (2024): 173558. https://doi.org/10.1016/j.scitotenv.2024.173558.
31. Xiao, Jianhua J, et al.. "Numerical simulation of the airflow at the world's largest concentrated solar power plant in a desert region." Solar Energy 232 (2022): 421-432. https://doi.org/10.1016/j.solener.2022.01.005.
32. Osman, Ahmedbahaaaldin Ibrahem Ahmed A, et al. "Extreme gradient boosting (Xgboost) model to predict the groundwater levels in Selangor Malaysia." Ain Shams Engineering Journal 12, no. 2 (2021): 1545-1556. https://doi.org/10.1016/j.asej.2020.11.011.
33. Yan, Hongyan H, et al.. "Investment estimation of prefabricated concrete buildings based on XGBoost machine learning algorithm." Advanced Engineering Informatics 54 (2022): 101789-101789. https://doi.org/10.1016/j.aei.2022.101789.
34. Hamilton, R. I. R, and Panagiotis N. P Papadopoulos. "Using SHAP Values and Machine Learning to Understand Trends in the Transient Stability Limit." IEEE Transactions on Power Systems 39, no. 1 (2023): 1384-1397. https://doi.org/10.1109/tpwrs.2023.3248941.
35. Kok, J. F., Parteli, E. J. R., Michaels, T. I., & Bou Karam, D. (2012). The physics of wind-blown sand and dust. Reports on Progress in Physics, 75(10), 106901. https://doi.org/10.1088/0034-4885/75/10/106901.
36. Jiang, Y., Gao, Y., He, C., Liu, B., Pan, Y., & Li, X. (2021). Spatiotemporal distribution and variation of wind erosion over the Tibetan Plateau based on a coupled land-surface wind-erosion model. Aeolian Research, 50, 100699. https://doi.org/10.1016/j.aeolia.2021.100699.
37. Fan, Y., Du, H., Han, Z., Liu, X., Liu, X., & Li, Z. (2024). Assessment of dust emissions and their controlling factors on the Hoh Xil, north-central part of the Qinghai-Tibetan plateau. Environmental and Sustainability Indicators, 24, 100487. https://doi.org/10.1016/j.indic.2024.100487.
38. Jinjiao, Hu ., Qingping, Zhou ., Quanheng, Cao ., & Jian, Hu. (2022). Effects of ecological restoration measures on vegetation and soil properties in semi-humid sandy land on the southeast Qinghai-Tibetan Plateau, China. Global Ecology and Conservation, 33, e02000. https://doi.org/10.1016/j.gecco.2022.e02000.
39. Mayaud, J. R., & Webb, N. P. (2017). Vegetation in Drylands: Effects on Wind Flow and Aeolian Sediment Transport. Land, 6(3), 64. https://doi.org/10.3390/land6030064.
40. Gholami, H., Darvishi, E., Moradi, N., Mohammadifar, A., Song, Y., Li, Y., Niu, B., Kaskaoutis, D., & Pradhan, B. (2024). An interpretable (explainable) model based on machine learning and SHAP interpretation technique for mapping wind erosion hazard. Environmental Science and Pollution Research, 31(56), 64628-64643. https://doi.org/10.1007/s11356-024-35521-x.
41. Jarrah, M., Mayel, S., Tatarko, J., Funk, R., & Kuka, K. (2020). A review of wind erosion models: Data requirements, processes, and validity. Catena, 187, 104388. https://doi.org/10.1016/j.catena.2019.104388.
42. Liu, Xiufan, Du, Heqiang, Liu, Xinlei, Fan, Yawei, Li, Sen, Wang, Tao, & Guo, Zichen. (2024). An improvement of the Revised Wind Erosion Equation by considering the effect of non-photosynthetic vegetation. Geoderma, 445, 116880. https://doi.org/10.1016/j.geoderma.2024.116880.
43. Yan, Y., Wang, X., Guo, Z., Chen, J., Xin, X., Xu, D., Yan, R., Chen, B., & Xu, L. (2018). Influence of wind erosion on dry aggregate size distribution and nutrients in three steppe soils in northern China. Catena, 170, 159-168. https://doi.org/10.1016/j.catena.2018.06.013.
44. Zhang, G.-F., Azorin-Molina, C., Chen, D., McVicar, T. R., Guijarro, J. A., Deng, K.-Q., Minola, L., Lee, J., Son, S.-W., Ma, H., & Shi, P.-J. (2024). Variability and trends of near-surface wind speed over the Tibetan Plateau: The role played by the westerly and Asian monsoon. Advances in Climate Change Research, 15(3), 525-536. https://doi.org/10.1016/j.accre.2024.04.007.